Composites Science and Technology 191 (2020) 108075

Contents lists available at ScienceDirect

Composites Science and Technology

journal homepage: http://www.elsevier.com/locate/compscitech

Mechanistic insights on ultra-tough polylactide-based ionic nanocomposites

Jean-Emile Potaufeux [a,b], Jérémy Odent [a], Delphine Notta-Cuvier [b], Rémi Delille [b], Sophie Barrau [c], Emmanuel P. Giannelis [d], Franck Lauro [b], Jean-Marie Raquez [a,*]

[a] Laboratory of Polymeric and Composite Materials (LPCM), Center of Innovation and Research in Materials and Polymers (CIRMAP), University of Mons (UMONS), Place du Parc 20, 7000, Mons, Belgium
[b] Laboratory of Industrial and Human Automatic Control and Mechanical Engineering (LAMIH), UMR CNRS 8201, University Polytechnique Hauts-De-France (UPHF), Le Mont Houy, 59313, Valenciennes, France
[c] Unité Matériaux et Transformations (UMET)−CNRS UMR 8207, Université Lille 1, 59655, Villeneuve d'Ascq, France
[d] Department of Materials Science and Engineering, Cornell University, Ithaca, NY, 14853, USA

ARTICLE INFO

Keywords:
Ionic network
Smart materials
Nano composites
Fracture toughness
Extrusion

ABSTRACT

We report the synthesis and characterization of ultra-tough polylactide-based ionic nanocomposites via melt-blending of commercial polylactide (PLA), imidazolium-functionalized poly(ethylene glycol)-based polyurethane (*im*-PU) and surface-modified sulfonated silica nanoparticles (SiO_2–SO_3H) using extrusion techniques. The proximity of bulky pendant imidazolium cationic sites attached onto the highly functionalized polyurethane to the anionic sulfonate groups at the silica nanoparticle surface readily allow maximizing dynamic ionic interactions within the resulting PLA-based materials. This new design leads to a unique property profile that combines ultra-toughness (no break) and ductility (up to 150%), without critical loss of stiffness as well as improved thermal stability (up to 40 °C higher compared to neat PLA). In addition, we present a detailed mechanistic study aiming at elucidating the energy-dissipative toughening in these PLA/*im*-PU/SiO_2–SO_3H blends under quasi-static and high-speed loadings (*ca.* impact, tensile, 3-points bending). Relying on Small-Angle X-Ray Scattering (SAXS), creep and rheological measurements, a toughening mechanism is finally proposed to account for the impact behavior of the resulting ionic nanocomposites.

1. Introduction

Dynamic polymer systems, whereby specific bonds or interactions can undergo reversible breaking and restoration under certain conditions offer exciting opportunities for the development of unique smart materials with tunable functionality. Shape-memory [1,2], self-healing [3,4], piezoelectric [5] or mechanochromic [6] materials have been developed, taking advantage of their ability to physically or chemically respond to an immediate environmental change. Dynamic systems can be classified into two categories, depending on the dynamic exchange mechanism involved, depicted as either dissociative or associative. The former exploits chemical bonds that break and then subsequently reform, while the later involves the breaking of the original crosslinks, together with the simultaneous creation of a new covalent bond to another anchoring point (meaning that the number of covalent bonds is constant) [7]. Leibler et al. developed the so-called vitrimers based on associative mechanisms, leading to thermosets combining high stiffness and recyclability at molten state [8]. However, side-reactions or degradation are usually induced during material processing at high temperature and thermosets cannot be easily reprocessed by traditional means. Numerous methods involving a variety of dissociative non-covalent dynamic interactions such as hydrogen bonding [9], Diels-Alder cycloaddition [4], π-π stacking [10], metal-ligand coordination [11–13] and ionic bonding [14] have been thereby utilized to create reprocessable physically crosslinked polymers. The latter is illustrated by Surlyn®, a commercial poly(ethylene-*co*-methacrylic acid)-based ionomer resin manufactured by Dupont™ [2]. Compared to other physical crosslinks, the dynamic and reversible nature of electrostatic interactions present in ionic systems offers the possibility to endow materials with enhanced dissipation of energy under mechanical testing [15–17], elastic recovery properties [18] or even uncommon strain-dependency [19]. As such, Mayumi and Long et al. [18,19] provided the stress-strain relation of model dual crosslink gels based on permanent and ionic transient crosslinks. Using a three-dimensional finite strain model, they ultimately proved that the gels show rate-dependent mechanical response, suggesting that improved

* Corresponding author.
E-mail address: jean-marie.raquez@umons.ac.be (J.-M. Raquez).

https://doi.org/10.1016/j.compscitech.2020.108075
Received 3 October 2019; Received in revised form 11 February 2020; Accepted 15 February 2020
Available online 17 February 2020

mechanical properties are closely tied up to the breaking and reattaching of the transient ionic crosslink present in the network. Likewise, Rose et al. [20] have focused on the time dependence of dissipative and recovery processes in nanohybrid hydrogels that combine a poly(*N, N*-dimethylacrylamide) covalent network and physical interactions by adsorption of polymer chains at the silica nanoparticle surface. Note that these physical crosslinks are further able to dissipate strain energy during their dynamic exchanges, thus delaying the macroscopic rupture of the material [21].

Building on the ionic motif, our group recently designed multi-responsive ionic nanocomposites that combine simultaneous improvement in stiffness, toughness and extensibility [14]. In addition, the nanocomposites exhibit unique strain-dependent behavior (*i.e.* the deformation increases with increasing strain rate) and return to the normal state after deformation including not only shape-memory but also self-healing behavior that were attributed to the dynamic and reversible nature of the ionic imidazolium-sulfonate interactions present in the system. In another approach, biosourced polylactide (PLA) was endowed with shape-memory properties by blending commercial PLA with imidazolium-terminated glassy PLA and rubbery poly[ε-caprolactone-*co*-D,L-lactide] oligomers and adding surface-modified silica nanoparticles [1]. The silica nanoparticles herein played a vital role in determining the overall material performance by creating temporary crosslinks between the polymer chains [22]. In the present contribution, we leverage the reversibility endowed to ionic systems specifically with the reinforcement effect provided by these nanoparticles to design ultra-tough PLA-based ionic nanocomposites with high-energy dissipation under quasi-static and high-speed loadings. It is worth recalling that the brittle nature of PLA is a perpetual challenge for its industrialization, which prompted us to investigate some of the potential advantages of introducing electrostatic interactions into the system. While extrusion techniques are preferred to solvent casting for its large-scale implementation, high electrostatic charge density are required to optimize the dynamics within the PLA-based materials [23,24]. Herein, poly (ethylene glycol) (PEG)-based additives have been demonstrated to be the ideal candidate for toughening brittle PLA. Integrating high molecular weight PEG-based *ionic* polyurethanes with pendant imidazolium cations (*im*-PU) and surface-modified sulfonate silica nanoparticles (SiO_2–*SO_3H*) into a conventional PLA matrix thereby appeared to us as a promising strategy to toughen PLA, while avoiding any plasticization effect related with low molecular oligomers. Besides, the dynamic nature of the ionic bonds present in the PLA-based nanocomposites provides an additional mechanism for toughening PLA over a wide range of strain rate. The present work further aims at establishing the mechanism of the energy-dissipative toughening as well as delineating the key parameters responsible for the final material performance. The system presented here represents a platform for designing more advanced PLA-based materials that would offer exciting opportunities for a wide range of applications including biomedical [25], packaging [26], textiles [27], automotive [28] or even 3D printing [29].

2. Experimental section

2.1. Materials

A commercially available extrusion-grade PLA (NatureWorks 4032D, Mn = 133,000 ± 5000 g mol^{-1}, Đ = 1.94 ± 0.06 as determined by size-exclusion chromatography and 1.4 ± 0.2% D-isomer content as provided by the supplier) was dried for 24h under vacuum at 70 °C. Hexamethylene diisocyanate (HMDI, >98%, Aldrich) was stored in a glove box. Polyethylene glycol (PEG, 2000 g mol^{-1}, Alfa Aesar), poly(ethylene glycol-*ran*-propylene glycol) (PEG-*ran*-PPG, 2500 g mol^{-1}, Sigma), 2,2-bis(bromomethyl)propane-1,3-diol (BBPDO, 98%, Sigma), 1-methylimidazole (99%, Aldrich), dibutyltin dilaurate (DBTDL, 95%, Sigma), Ludox HS30 colloidal silica (mean diameter 18 nm, Aldrich), 3-(hydroxysilyl)-1-propane sulfonic acid (SIT, 40 wt%, Gelest), sodium hydroxide solution (1M, Aldrich), anhydrous tetrahydrofuran (THF, >99.8%), anhydrous *N,N*-dimethylformamide (DMF, >99.7%, Alfa Aesar), diethyl ether (>99%, Aldrich), Ultranox®626 (Chemtura) were used without further purification.

2.2. PLA-based ionic nanocomposite preparation

Imidazolium-functionalized poly(ethylene glycol)-based polyurethane (*im*-PU) made of semi-crystalline PEG ($M_n \approx 107{,}000$ g mol^{-1}, Đ ≈ 3.0, yield ≈ 95%) or amorphous PEG-*ran*-PPG ($M_n \approx 111{,}000$ g mol^{-1}, Đ ≈ 2.3, yield ≈ 96%) and sulfonate functionalized silica nanoparticles (*ca.* 17 ± 5 nm of diameter, 1 ± 0.1 mmol of SO_3H/g of silica) were prepared according to a previously reported procedure [14]. The as-synthesized *im*-PU is dissolved in deionized water followed by the dropwise addition of the sulfonate silica suspension under stirring, sonication and freeze-drying to form ionic *im*-PU/SiO_2–*SO_3H* hybrids. The resulting ionic materials were subsequently melt-blended with PLA at 180 °C and 60 rpm for 5 min under nitrogen using a twin-screw micro-compounder (15 cm^3). The resulting PLA-based ionic nanocomposites were shaped into specimens of various geometries by compression molding at 180 °C using the following procedure: no pressure for 2 min, followed by 3 degassing steps and 1 min under 10 bars.

2.3. Characterization techniques

Proton nuclear magnetic resonance (1H NMR) spectra were recorded in DMSO, using a Bruker AMX-500 spectrometer at a frequency of 500 MHz. Size-exclusion chromatography (SEC) were carried out on an Agilent 1200 apparatus in THF (containing 2 wt% of NEt_3). Samples in solution (1 mg mL^{-1}) were injected with a 1 mL min^{-1} flow rate at 35 °C in a pre-column PL gel 10 mm (50 × 7.5 mm) followed by two gradient columns PL gel 10 mm mixed-B (300 × 7.5 mm). Molecular weights and molecular weight distributions were calculated by reference to a relative calibration curve made of polystyrene standards. Rheological measurements were performed using an Anton Paar Rheometer MCR-302 using a plate-plate geometry system with a 25 mm diameter. Frequency sweep measurements were performed at 60 °C for the ionic *im*-PU/SiO_2–*SO_3H* systems and at 180 °C for the resulting ionic PLA/*im*-PU/SiO_2–*SO_3H* nanocomposites with a strain of 1% (linear viscoelastic regime) and a frequency range between 0.01 Hz and 100 Hz. Creep-recovery experiments were further used to measure the elasticity of the material. A constant shear stress of 50 Pa was applied for 300s followed by a recovery of 600s, when the shear stress is set back to zero. Small Angle X-ray Scattering (SAXS) experiments were carried out using a Xeuss 2.0 (XENOCS) with a GeniX3D microsource (λ = 1.54 Å). The sample-to-detector distance was 1001 mm. Dynamic mechanical thermal analyses (DMTA) were performed under ambient atmosphere using a DMTA Q800 apparatus from TA Instruments in a dual cantilever mode. The measurements were carried out at a constant frequency of 1 Hz, an amplitude of 20 μm and a temperature range from −80 °C to 150 °C at a heating rate of 2 °C.min^{-1}. Tensile tests were carried out on a Zwick universal tensile testing machine (speed = 1 mm min^{-1}, preload = 5N) according to ASTM D638. The volume energy of deformation is defined as $E_{def} = \int_0^{\varepsilon_{break}} \sigma.d(\varepsilon)$, where σ is the nominal stress and ε the nominal strain. Notched Izod impact tests were performed according to ASTM D256 using a Ray-Ran 2500 pendulum impact tester (mass = 0.668 kg, speed = 0.46 m s^{-1}, E = 4J). Room-temperature impact-fractured surfaces of samples were analyzed through a transmission electron microscopy (TEM) using a Philips CM20 microscope operated at 200 kV. For recording TEM images, the samples were ultra-cryomicrotomed at −100 °C by a Leica UCT microtome. ImageJ software was used to analyze the morphological structures on TEM images and estimate the particles and microdomains sizes within the matrix. 3-points bending tests were performed at room temperature on pre-notched samples at

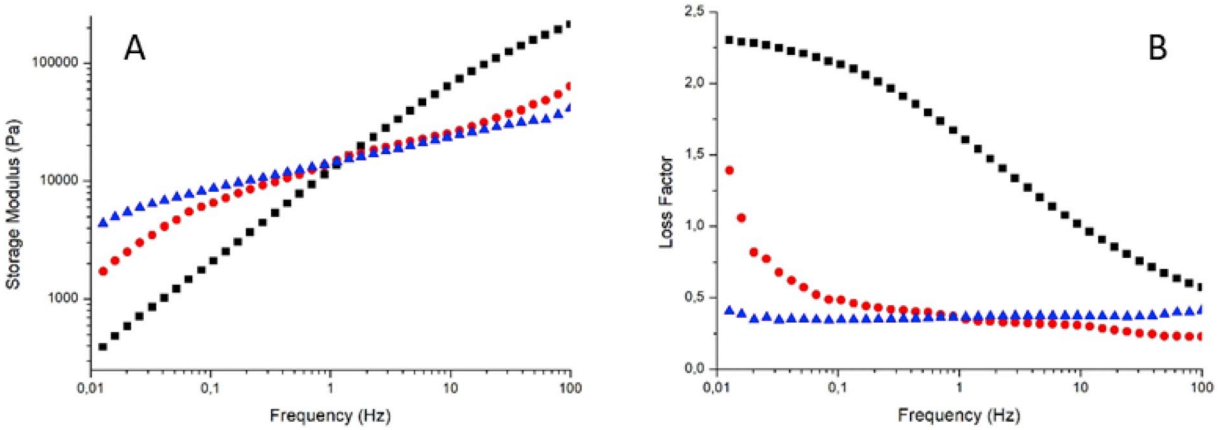

Fig. 1. (**A**) Storage modulus and (**B**) loss factor as a function of frequency of neat *im*-PU (made of PEG-*ran*-PPG building blocks) (black squares) and resulting ionic *im*-PU/SiO_2–SO_3H systems containing 10 wt% (red circles) and 20 wt% (blue triangles) of SiO_2–SO_3H. (For interpretation of the references to colour in this figure legend, the reader is referred to the Web version of this article.)

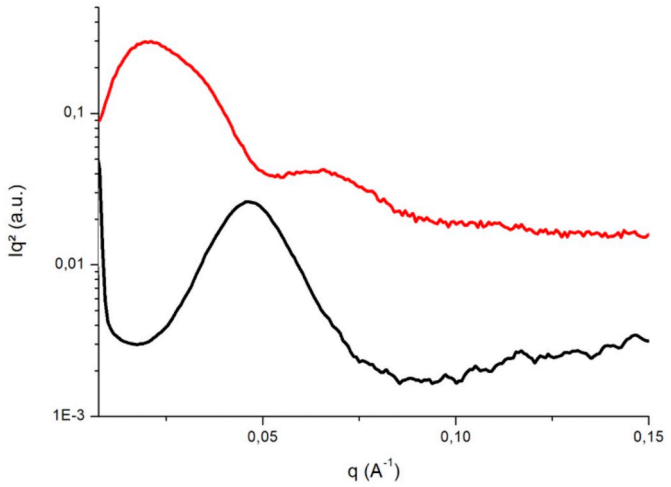

Fig. 2. SAXS measurements of neat *im*-PU (made of PEG building blocks) network (black curve), and resulting ionic *im*-PU/SiO_2–SO_3H systems containing 10 wt% of SiO_2–SO_3H (red curve). (For interpretation of the references to colour in this figure legend, the reader is referred to the Web version of this article.)

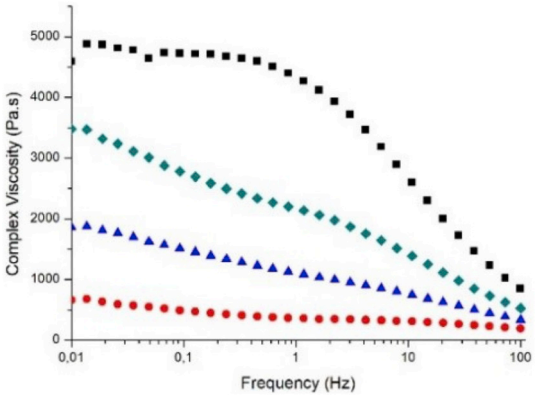

Fig. 3. Complex viscosity η* as a function of frequency of neat PLA (black squares), PLA containing 20 wt% of *im*-PU (made of PEG-*ran*-PPG building blocks) (red circles) and resulting ionic PLA-based nanocomposites containing 20 wt% of *im*-PU/SiO_2–SO_3H (90/10 wt%) (blue triangles) or 20 wt% of *im*-PU/SiO_2–SO_3H (80/20 wt%) (green diamonds). (For interpretation of the references to colour in this figure legend, the reader is referred to the Web version of this article.)

displacement rates of 0.1 mm min^{-1} (*ca.* quasi-static mode) and 100 mm min^{-1} (*ca.* high speed mode) using an Instron E3000 electromagnetic tensile machine and cameras at a frame rate of 0.5 fps or 200 fps for the lowest or highest test speed, respectively. Fracture surfaces of specimens were sputter-coated with gold and then analyzed through scanning electron microscopy (SEM) using a Philips XL20 microscope (1–30 kV). Thermal gravimetric analysis (TGA) was performed using a TGA Q500 from TA Instruments at a heating rate of 20 °C.min^{-1} from room temperature to 800 °C, under nitrogen flow.

3. Results and discussion

The design of ultra-tough polylactide (PLA)-based materials relies on the close vicinity of the cationic imidazolium rings to the anionic sulfonate groups [30]. Fabrication of the new PLA-based ionic hybrids is based on blends obtained from commercial PLA with imidazolium-functionalized PEG-based polyurethanes (*im*-PU) and surface-modified sulfonate silica nanoparticles (SiO_2–SO_3H) using solvent-free extrusion techniques. Since the imidazolium groups are randomly distributed along the polyurethane backbone at high concentration (*i.e.* 10 mol%), we can expect that all the imidazolium rings

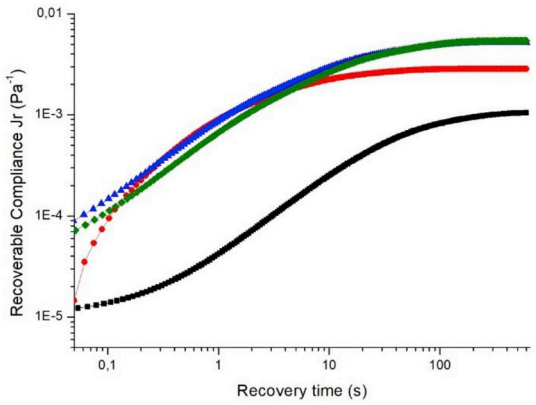

Fig. 4. Recoverable compliance after creep experiments of neat PLA (black squares), PLA containing 20 wt% of *im*-PU (made of PEG-*ran*-PPG building blocks) (red circles) and resulting ionic PLA-based nanocomposites containing 20 wt% of *im*-PU/SiO_2–SO_3H (90/10 wt%) (blue triangles) or 20 wt% of *im*-PU/SiO_2–SO_3H (80/20 wt%) (green diamonds). (For interpretation of the references to colour in this figure legend, the reader is referred to the Web version of this article.)

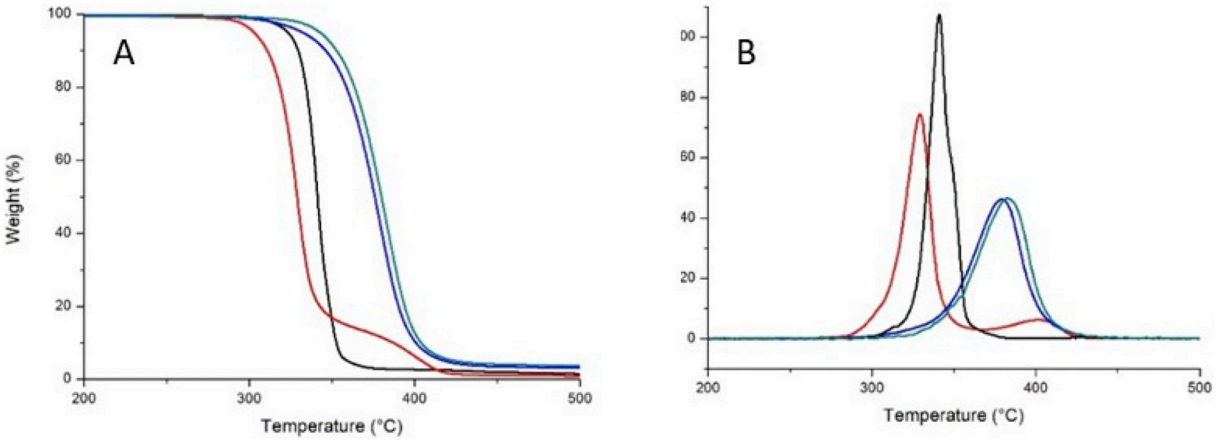

Fig. 5. (**A**) Thermogravimetric analyzes (TGA) and (**B**) derivative (DTGA) of neat PLA (black), PLA containing 20 wt% of *im*-PU (made of PEG-*ran*-PPG building blocks) (red) and resulting ionic PLA-based nanocomposites containing 20 wt% of *im*-PU/SiO_2–SO_3H (90/10 wt%) (blue) or 20 wt% of *im*-PU/SiO_2–SO_3H (80/20 wt %) (green). (For interpretation of the references to colour in this figure legend, the reader is referred to the Web version of this article.)

Table 1
Mechanical properties of neat PLA, binary PLA/SiO_2–SO_3H and PLA/*im*-PU (made of PEG-*ran*-PPG building blocks) blends and resulting ionic ternary PLA/*im*-PU/SiO_2–SO_3H-based nanocomposites.

Composition [wt%]	E [GPa]	σ_y [MPa]	ε_b [%]	E_{def} [MPa]	IS [kJ/m^2]
PLA	3.1 ± 0.1	61 ± 8	3 ± 0.5	1.1 ± 0.1	3 ± 0.5
PLA + 2% SiO_2–SO_3H	3.3 ± 0.1	61 ± 2	2.5 ± 0.5	0.9 ± 0.1	3 ± 0.5
PLA + 10% *im*-PU	2.7 ± 0.1	40 ± 3	62 ± 7	10 ± 1	4.3 ± 0.4
PLA + 10% *im*-PU/SiO_2–SO_3H (90/10)[a]	2.7 ± 0.1	39 ± 1	72 ± 15	12 ± 1	5.5 ± 0.5
PLA + 10% *im*-PU/SiO_2–SO_3H (80/20)[b]	2.7 ± 0.1	34 ± 0.1	100 ± 22	24 ± 2	7 ± 1
PLA + 20% *im*-PU	2.2 ± 0.1	29 ± 2	64 ± 9	11 ± 1	12 ± 1
PLA + 20% *im*-PU/SiO_2–SO_3H (90/10)[c]	2.3 ± 0.1	28 ± 1	75 ± 12	13 ± 2	**No Break**
PLA + 20% *im*-PU/SiO_2–SO_3H (80/20)[d]	2.3 ± 0.1	27 ± 1	142 ± 38	26 ± 5	**No Break**

E: Young's modulus; σ_y: Yield stress; ε_b: Strain at break; E_{def}: Volume energy of deformation; IS: Impact strength.
[a] This blend is referred as 90 wt% PLA, 9 wt% *im*-PU, 1 wt% SiO_2–SO_3H.
[b] This blend is referred as 90 wt% PLA, 8 wt% *im*-PU, 2 wt% SiO_2–SO_3H.
[c] This blend is referred as 80 wt% PLA, 18 wt% *im*-PU, 2 wt% SiO_2–SO_3H.
[d] This blend is referred as 80 wt% PLA, 16 wt% *im*-PU, 4 wt% SiO_2–SO_3H.

are largely accessible to the sulfonate groups around the silica nanoparticles, therefore maximizing the electrostatic interactions in the system. Prior to introducing the ionic *im*-PU/SiO_2–SO_3H systems into the PLA matrix, rheological measurements were used to monitor the formation of the dynamic ionic network. At low frequencies, the storage modulus increases by several order of magnitude upon the addition of SiO_2–SO_3H into *im*-PU (see Fig. 1 for PEG-*ran*-PPG-based *im*-PU and Fig. S1 for corresponding PEG-based *im*-PU). The loss factor tan(δ) is frequently independent from 10 to 20 wt% of SiO_2–SO_3H, confirming the creation of an extensive 3D network of silica nanoparticles within the material for these loadings [31]. Note that the theoretical charge balance (*i.e.* 1:1 ratio of sulfonate: imidazolium) is achieved at about 10 wt% of SiO_2–SO_3H. Since not all the sulfonate groups onto the silica surface are accessible to the imidazolium groups along the polymer chains, higher content of silica nanoparticles (from 10 to 20 wt%) is required maximizing the electrostatic interactions in the system. Small Angle X-Ray scattering (SAXS) experiments were performed to further characterize the system. Fig. 2 shows the Lorentzian representation of integrated intensity profiles I(q). While the ionic systems based on *im*-PU made from amorphous PEG-*ran*-PPG are characterized by broad peaks, the ones made of semi-crystalline PEG show better crystallographic characteristics (Fig. 2). A maximum peak observed at 0.045 $Å^{-1}$ is due to the average long period (L_p) of PEG building blocks, *i.e.* the regular stacking of the amorphous and crystalline layers. Using Bragg's equation [32] ($L_p = 2\pi/q_{max}$) and the position of the maximum peak, we can estimate L_p at *ca.* 13.4 nm. Adding 10 wt% of SiO_2–SO_3H into *im*-PU made of PEG building blocks leads to three scattering peaks at 0.021, 0.033 and 0.066 A^{-1}, respectively. Peaks at 0.033 and 0.066 A^{-1} are due to the silica nanoparticles. Fitting I(q) with a Gaussian function led to a particle radius of 17.3 nm and size distribution of 7.4 nm, which is consistent with monodisperse silica nanoparticles of *ca.* 17 nm. The SAXS data suggests that the electrostatic interactions are critical in order to achieve a good nanoparticle dispersion. Furthermore, the addition of silica nanoparticles shifts the ascribed to *im*-PU characteristic length from 0.045 A^{-1} to 0.021 A^{-1}, which correspond to ~13.4 nm and 31 nm for neat *im*-PU and the ionic *im*-PU/SiO_2–SO_3H systems, respectively. The difference of ~17 nm is attributed to the contribution of silica nanoparticles (*ca.* 17 ± 5 nm of diameter) in the long-periodicity, reinforcing the critical importance of ionic interactions for achieving a good dispersion.

After confirming the critical nature of ionic interactions between imidazolium and sulfonate groups, the resulting ionic systems (*i.e. im*-PU/SiO_2–SO_3H at 90/10 and 80/20 wt%) were subsequently melt-blended with PLA using extrusion techniques. Recall that ionic *im*-PU/SiO_2–SO_3H systems are maximizing Coulomb interactions at 90/10 and 80/20 wt%, which should in turn endow the resulting PLA-based nanocomposites with dynamic behavior. Rheological measurements show that adding 20 wt% of ionic *im*-PU/SiO_2–SO_3H systems into commercial PLA leads to a significant increase of the storage modulus (Fig. S2) and the complex viscosity (Fig. 3) in the lower frequency regime, confirming the establishment of an extensive 3D particle network within the ionic PLA-based nanocomposite. The ability of the

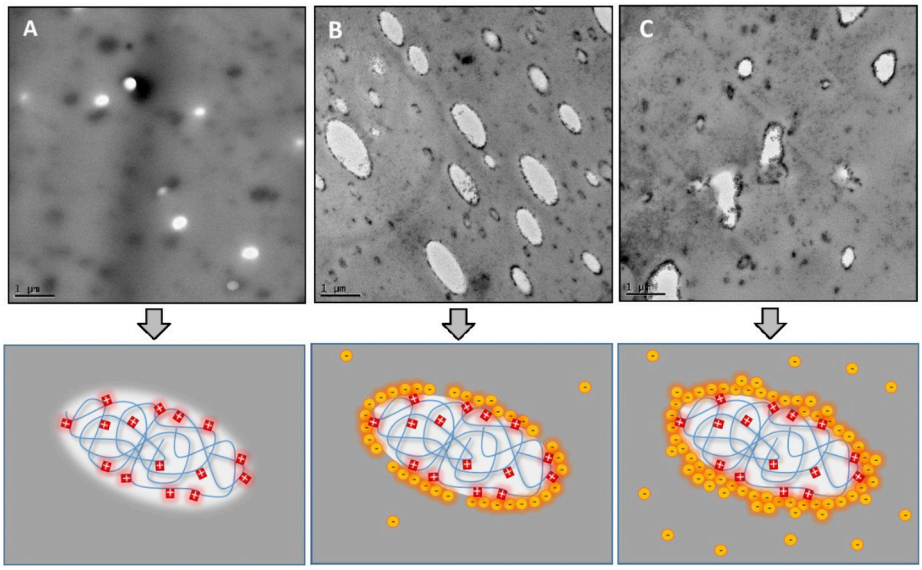

Fig. 6. TEM images and schematic representations of the morphologies (white part represents the *im*-PU nodules, red squares are the cationic imidazolium rings and yellow circles are the anionic sulfonate functionalized silica nanoparticles) of (**A**) PLA containing 20 wt% of *im*-PU (made of PEG-*ran*-PPG building blocks) and resulting ionic PLA-based nanocomposites containing (**B**) 20 wt% of *im*-PU/SiO_2–SO_3H (90/10 wt%) or (**C**) 20 wt% of *im*-PU/SiO_2–SO_3H (80/20 wt%). (For interpretation of the references to colour in this figure legend, the reader is referred to the Web version of this article.)

PLA nanocomposites to dissipate energy is compared to neat PLA using creep-experiments (Fig. 4). The recoverable compliance increases with the recovery time for neat PLA, showing an inflection point at intermediate recovery times (*ca.* 5s). The addition of either *im*-PU or ionic *im*-PU/SiO_2–SO_3H systems increases the elastic compliance of the PLA matrix consistent with the final blend viscosity. Note that the steady-state elastic compliance increases as the amount of SiO_2–SO_3H increases into the hybrids, thanks to the ability of the ionic network to dissipate energy. Furthermore, while the simple PLA/*im*-PU blends show no inflection point, the creation of temporary ionic crosslinks upon the addition of SiO_2–SO_3H into PLA/*im*-PU blends leads to an inflection point at short recovery times (*ca.* 0.1s).

Odent et al. attribute the mechanism by which the ionic systems dissipate strain energy to the dissociation dynamics of the ionic crosslinks as well as motion of the nanoparticles under applied stress [14]. Dynamic mechanical thermal analysis (DMTA) was thereby used to investigate the molecular mobility of the system (Fig. S3). While neat PLA is characterized by an apparent alpha transition (Tα) of *ca.* 56 °C, PLA/*im*-PU (made of PEG-*ran*-PPG building blocks) blends show two distinct peaks at *ca.* −59 °C and 53 °C, which are attributed to *im*-PU and PLA matrix, respectively. Adding SiO_2–SO_3H into these blends shifts the characteristic Tα peak of *im*-PU towards lower temperatures, while the characteristic Tα peak of PLA shifts towards higher temperatures (the difference of temperature ΔT is about 7 °C). We attribute this behavior to the limited mobility of silica nanoparticles at the molecular level. We believe, even though, that the nanoparticles are mobile enough to create temporary crosslinks between the polymer chains, which in turn result in large energy dissipation. Herein, creep-experiments using DMTA readily allow attesting for the large energy dissipation when the stress is released (Fig. S4). Note that the use of high molecular weights *im*-PU clearly limit the plasticization extent of the PLA commonly observed in the case of melt-blending of PLA-based systems. As far as the creation of ionic *im*-PU/SiO_2–SO_3H crosslinks within PLA could largely improve its thermal stability, thermal investigations are also required in this work (Fig. 5). Note that the simple addition of sulfonated silica nanoparticles within PLA led to a reduced reprocessability if not neutralized by the proximity of imidazolium cationic groups. In contrast, a two-step degradation at *ca.* 329 °C and *ca.* 402 °C respectively attributed to the continuous PLA matrix and the dispersed *im*-PU phase is recorded for the simple PLA/*im*-PU blends. Further loading SiO_2–SO_3H into the PLA/*im*-PU blends significantly shift the degradation processes to higher temperatures. For instance, an increase of *ca.* 42 °C is recorded for the resulting ionic PLA-based nanocomposites containing 20 wt% of *im*-PU/SiO_2–SO_3H (80/20 wt%) compared to neat PLA (*i.e.* from 341 °C to 383 °C). We believe that silica nanoparticles act as interfacial compatibilizers, strengthening the adhesion between polymer components which in turn allow high thermal stability. Note that weight losses are also consistent with the blend composition of resulting PLA-based materials and that the dynamic and reversible nature of the ionic imidazolium-sulfonate interactions present in the system allow enhanced reprocessability, while degradation is usually more prone to occur at high temperature during material processing.

In our design, we envisioned that the dissociation dynamics of the ionic crosslinks should allow fine-tuning of the overall material performances. To that end, tensile and impact properties of the ionic PLA-based nanocomposites were determined and compared to neat PLA as well as binary PLA/SiO_2–SO_3H and PLA/*im*-PU blends (Table 1). Note that while we focus on the simplicity about the PLA-based ionic hybrids based on the amorphous PEG-*ran*-PPG-based *im*-PU, the corresponding systems made of semi-crystalline PEG-based *im*-PU show similar trends (Table S1). The neat PLA behaves as a stiff and glassy material with a high Young's modulus of 3.1 GPa, a strain at break of 3% and an impact strength of 3 kJ/m^2. The simple addition of SiO_2–SO_3H within PLA resulted in a decrease in elongation at break (2.5%) but an increase in Young's modulus (3.3 GPa) together with no change in impact strength (3 kJ/m^2). When 10 or 20 wt% of *im*-PU is blended within PLA, a decrease of the Young's modulus (*ca.* 2.2 MPa) together with an increase of strain at break (*ca.* 64%) are seen. Addition of SiO_2–SO_3H within such PLA/*im*-PU blends improves significantly the overall material performance. For instance, the ionic PLA nanocomposites containing 20 wt% of *im*-PU/SiO_2–SO_3H (80/20 wt%) show a strain at break of 142%, together with a Young's modulus of *ca.* 2.3 MPa. This is a remarkable behavior as improvements in modulus in most nanocomposite systems are typically accompanied by a decrease in strain at break. The most striking feature concerns the significant increase in the dissipated deformation energy (obtained from tensile testing, *i.e.* quasi-static strain rate) and the impact strength (obtained from impact testing, *i.e.* high strain rate) of the ionic PLA nanocomposites (Table 1). Under quasi-static loadings (*i.e.* slow strain rate), we see that the dynamic ionic crosslinks relax, so that the progressive breaking and restoration of the ionic linkages allow the new ionic nanocomposites to sustain high levels of strain (Fig. S5). As a result, the volume energy of deformation increases from 1.1 MPa for neat PLA, 0.9 MPa for binary PLA/SiO_2–SO_3H blend and 11 MPa for the non-ionic PLA/*im*-PU blends to 26 MPa for the ionic nanocomposites containing 20 wt% of *im*-PU/SiO_2–SO_3H (80/20 wt%). While such a loading (20 wt% of *im*-PU/SiO_2–SO_3H) is surely the

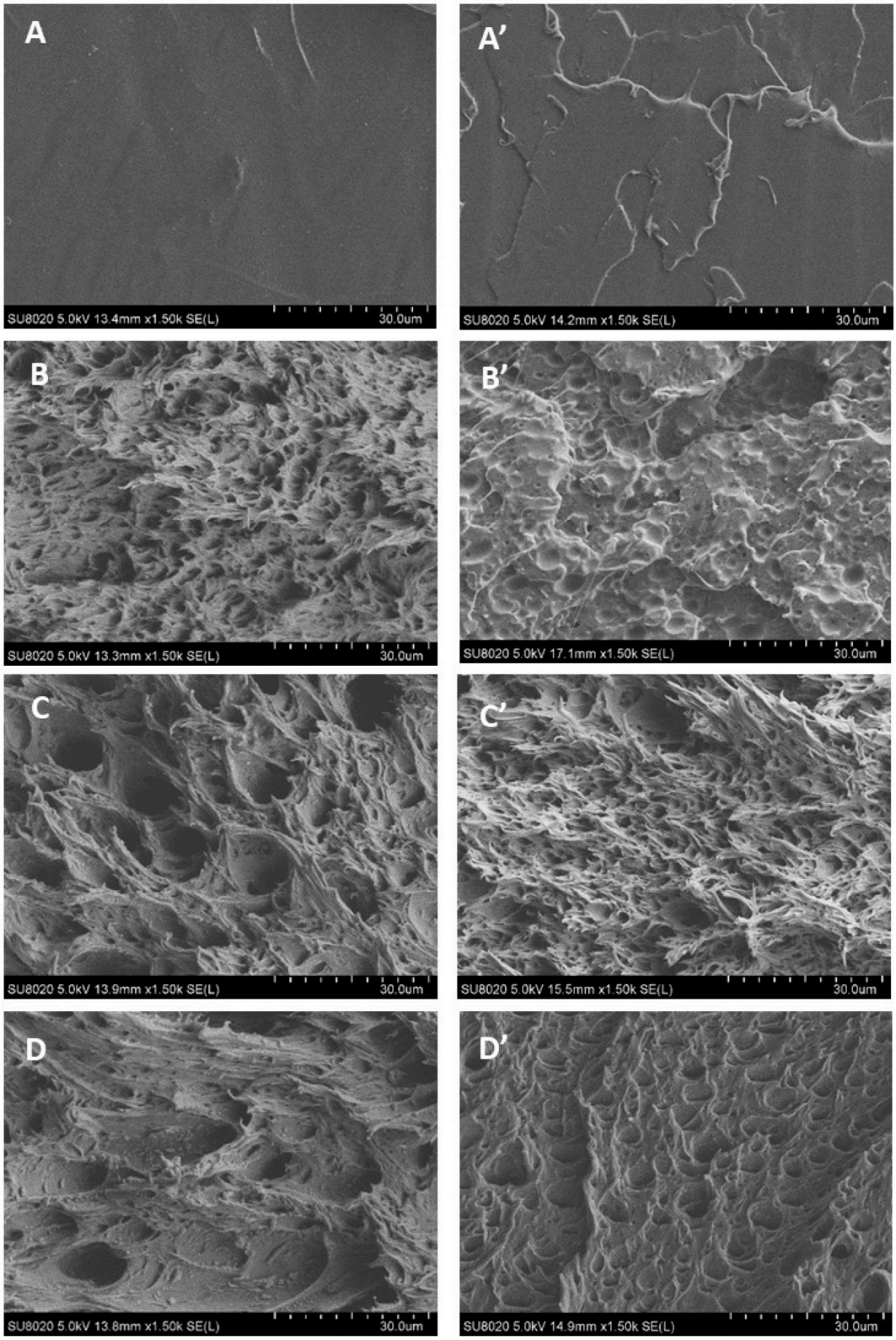

Fig. 7. SEM images of room-temperature fractured surfaces of (**A, A′**) neat PLA, (**B, B′**) PLA containing 20 wt% of *im*-PU (made of PEG-*ran*-PPG building blocks) and resulting ionic PLA-based nanocomposites containing (**C, C′**) 20 wt% of *im*-PU/SiO_2–SO_3H (90/10 wt%) or (**D, D′**) 20 wt% of *im*-PU/SiO_2–SO_3H (80/20 wt%) under quasi-static (**A, B, C, D**) and high loadings (**A′, B′, C′, D′**).

best compromise between high performance and degradation, lower loadings also provide mechanical reinforcement with a Young's modulus of *ca.* 2.7 MPa, a strain at break of *ca.* 100% and an impact strength of *ca.* 24 kJ/m^2 at 10 wt% of *im*-PU/SiO_2–*SO_3H* (80/20 wt%) within PLA.

We also predicted that the dissociation dynamics of ionic crosslinks should enable large energy dissipation under high loadings (*i.e.* under impact testing), as previously reported by Rose et al. [20]. A brittle-to-ductile transition characterized by a 4-fold increase in impact strength (12 ± 1 kJ/m^2) is seen for the simple blends containing 20 wt% of *im*-PU in PLA. On the other hand, no break (IS $>$ 60 kJ/m^2) under impact testing is observed in the case of the ionic PLA nanocomposites. Recall that the inherent brittleness of PLA is a perpetual challenge for its large-scale industrial implementation. Although a more detailed analysis to relate the strain-dependent behavior with the dynamic nature of the system might be needed, our results already suggest, in good agreement with recent investigations by Mayumi et al. [18], that transient ionic crosslinks are able to dissipate energy under a large range of deformation rate and for different kinds of mechanical loadings.

Transmission electron microscopy (TEM) analyses revealed cavities attributed to the dispersed immiscible *im*-PU within the PLA matrix (Fig. 6). In the ionic nanocomposites the major fraction of silica nanoparticles is specifically located at the PLA/*im*-PU interface, strengthening the interfacial adhesion between the polymeric components and, therefore, the overall material performances [22]. Note, though, that silica nanoparticles are not exclusively located at the PLA/*im*-PU interface and could be partly found within each polymeric partners (*i.e.* PLA matrix and *im*-PU microdomains). The morphologies of all nanocomposite samples are consistent with maximizing electrostatic interactions between the sulfonate and imidazolium groups on the silica and PU chains, respectively. It is worth noting that a microdomain size between ~700 and 900 nm is usually a precondition to efficiently toughen PLA-based materials [22,33]. In the ionic nanocomposites the mean size of the dispersed microdomains increases from ~250 nm to 500 nm, *i.e.* a 2-fold increase, upon the addition of SiO_2–*SO_3H*. Starting from its optimum microdomain average size, the emergence of great energy dissipative toughening mechanisms (referred as crazing, shear-yielding and debonding) becomes possible [24].

Scanning electron microscopy (SEM) of room-temperature fractured surfaces of the samples is shown in Fig. 7. While the brittle PLA matrix displays a very limited plastic deformation, high deformations and plasticity are evidenced in the PLA-based materials (Fig. S6). Stress whitening is widely observed under quasi-static (*i.e.* 0.1 mm/min) and high loading (*i.e.* 100 mm/min). This is due to the classical role of the dispersed phase acting as local stress concentrators at many sites throughout the material and initiating elementary toughening mechanisms. While crazing is responsible for the brittle character of PLA (Fig. 6a), localized zones of micro-voids and micro-fibrils are found upon the addition of *im*-PU within the PLA matrix, which contribute to enhanced crazing upon deformation (Fig. 7b). Addition of SiO_2–*SO_3H* to form the nanocomposites contributes to other energy-dissipative mechanisms, promoting shear band nucleation upon increasing deformation (Fig. 7c–d). The capacity of shear bands to stabilize craze growth thereby leads to improved energy dissipation before rupture. It may be that the specific localization of silica nanoparticles at the PLA/*im*-PU interface strengthens the adhesion between polymer components, promoting interfacial cavitation under stress by a so-called debonding mechanism. Note, however, that moving from quasi-static (*i.e.* 0.1 mm/min) to high loading (*i.e.* 100 mm/min) does not seem to provide a greater energy-dissipative toughening mechanism (Fig. S6). Yet, we believe the dissociation dynamics of the ionic crosslinks are responsible for toughening resulting ionic PLA-based nanocomposites.

4. Conclusions

Ultra-tough PLA-based ionic nanocomposites that leverage the reversible character of ionic bonds with the reinforcing effect of nanoparticles were demonstrated. The new materials are made of imidazolium-functionalized PEG-based polyurethanes (*im*-PU) and surface-modified sulfonate silica nanoparticles (SiO_2–*SO_3H*) blended with commercial PLA using melt extrusion. The presence of the ionic domains all along the polymer chains based on the cationic imidazolium rings on the complementary polymer interacting with the anionic sulfonate groups on silica endow the resulting nanocomposites with ultra-toughness (no break on impact) and ductility (up to 150%) without critical loss of stiffness as well as improved thermal stability (40 °C higher than the neat PLA). SAXS and rheological analyses confirmed the presence of ionic imidazolium-sulfonate interactions as well as the creation of an extensive 3D network of silica nanoparticles within the materials. The work presented evidence for the toughening mechanism related to the final mechanical performance. As expected, the ionic nanocomposites can undergo one or a combination of the most dissipative toughening mechanisms, namely the occurrence of crazing and shear-yielding, which promote high deformation and plasticity under quasi-static and high loadings compared to the neat PLA. Finally, the overall material performance was attributed to the dissociation dynamics of the ionic crosslinks in the system.

Declaration of competing interest

The authors declare that they have no known competing financial interests or personal relationships that could have appeared to influence the work reported in this paper.

CRediT authorship contribution statement

Jean-Emile Potaufeux: Conceptualization, Investigation, Writing - original draft, Writing - review & editing, Visualization. **Jérémy Odent:** Conceptualization, Writing - review & editing. **Delphine Notta-Cuvier:** Conceptualization, Writing - review & editing. **Rémi Delille:** Methodology, Investigation. **Sophie Barrau:** Investigation, Formal analysis. **Emmanuel P. Giannelis:** Resources. **Franck Lauro:** Conceptualization, Supervision. **Jean-Marie Raquez:** Conceptualization, Supervision.

Acknowledgements

The authors gratefully acknowledge support from both the Wallonia and the European Commission "FSE and FEDER" in the frame of LCFM-BIOMASS project as well as the National Fund for Scientific Research (F.R.S.-FNRS) and the European Union's Horizon 2020 research and innovation program under the BIODEST project (ID: 778092). J.-M. Raquez is 'Chercheur qualifié' by the F.R.S.-F.N.R.S. LAMIH authors are grateful to CISIT, the Hauts de France Region, the European Community, the Regional Delegation for Research and Technology, the Ministry of Higher Education and Research and the National Center for Scientific Research for their financial support.

Appendix A. Supplementary data

Supplementary data to this article can be found online at https://doi.org/10.1016/j.compscitech.2020.108075.

References

[1] J. Odent, J.-M. Raquez, C. Samuel, S. Barrau, A. Enotiadis, P. Dubois, E. P. Giannelis, Shape-memory behavior of polylactide/silica ionic hybrids, Macromolecules 50 (2017) 2896–2905, https://doi.org/10.1021/acs.macromol.7b00195.

[2] R. Dolog, R.A. Weiss, Properties and shape-memory behavior of compounds of a poly(ethylene- co -methacrylic acid) ionomer and zinc stearate, Polymer 128 (2017) 128–134, https://doi.org/10.1016/j.polymer.2017.09.010.

[3] J. Kang, D. Son, G.-J.N. Wang, Y. Liu, J. Lopez, Y. Kim, J.Y. Oh, T. Katsumata, J. Mun, Y. Lee, L. Jin, J.B.-H. Tok, Z. Bao, Tough and water-insensitive self-healing

elastomer for robust electronic skin, Adv. Mater. (2018), 1706846, https://doi.org/10.1002/adma.201706846.
[4] B. Willocq, F. Khelifa, J. Brancart, G. Van Assche, Ph Dubois, J.-M. Raquez, One-component Diels–Alder based polyurethanes: a unique way to self-heal, RSC Adv. 7 (2017) 48047–48053, https://doi.org/10.1039/C7RA09898G.
[5] A. Hänninen, E. Sarlin, I. Lyyra, T. Salpavaara, M. Kellomäki, S. Tuukkanen, Nanocellulose and chitosan based films as low cost, green piezoelectric materials, Carbohydr. Polym. 202 (2018) 418–424, https://doi.org/10.1016/j.carbpol.2018.09.001.
[6] A. Ruiz de Luzuriaga, J.M. Matxain, F. Ruipérez, R. Martin, J.M. Asua, G. Cabañero, I. Odriozola, Transient mechanochromism in epoxy vitrimer composites containing aromatic disulfide crosslinks, J. Mater. Chem. C 4 (2016) 6220–6223, https://doi.org/10.1039/C6TC02383E.
[7] W. Denissen, J.M. Winne, F.E. Du Prez, Vitrimers: permanent organic networks with glass-like fluidity, Chem. Sci. 7 (2016) 30–38, https://doi.org/10.1039/C5SC02223A.
[8] M. Capelot, D. Montarnal, F. Tournilhac, L. Leibler, Metal-catalyzed transesterification for healing and assembling of thermosets, J. Am. Chem. Soc. 134 (2012) 7664–7667, https://doi.org/10.1021/ja302894k.
[9] A.M. Grande, J.C. Bijleveld, S.J. Garcia, S. van der Zwaag, A combined fracture mechanical – rheological study to separate the contributions of hydrogen bonds and disulphide linkages to the healing of poly(urea-urethane) networks, Polymer 96 (2016) 26–34, https://doi.org/10.1016/j.polymer.2016.05.004.
[10] S. Shinde, J.L. Sartucci, D.K. Jones, N. Gavvalapalli, Dynamic π-conjugated polymer ionic networks, Macromolecules 50 (2017) 7577–7583, https://doi.org/10.1021/acs.macromol.7b01896.
[11] Y. Hui, Z.-B. Wen, F. Pilate, H. Xie, C.-J. Fan, L. Du, D. Liu, K.-K. Yang, Y.-Z. Wang, A facile strategy to fabricate highly-stretchable self-healing poly(vinyl alcohol) hybrid hydrogels based on metal–ligand interactions and hydrogen bonding, Polym. Chem. 7 (2016) 7269–7277, https://doi.org/10.1039/C6PY01752E.
[12] J. Liu, Y. Liu, Y. Wang, J. Zhu, J. Yu, Z. Hu, Disulfide bonds and metal-ligand co-crosslinked network with improved mechanical and self-healing properties, Mater. Today Commun. 13 (2017) 282–289, https://doi.org/10.1016/j.mtcomm.2017.10.013.
[13] I. Azcune, I. Odriozola, Aromatic disulfide crosslinks in polymer systems: self-healing, reprocessability, recyclability and more, Eur. Polym. J. 84 (2016) 147–160, https://doi.org/10.1016/j.eurpolymj.2016.09.023.
[14] J. Odent, J.-M. Raquez, Ph Dubois, E.P. Giannelis, Ultra-stretchable ionic nanocomposites: from dynamic bonding to multi-responsive behavior, J. Mater. Chem. A. 5 (2017) 13357–13363, https://doi.org/10.1039/C7TA04101B.
[15] J. Yang, M. Ma, X. Zhang, F. Xu, Elucidating dynamics of precoordinated ionic bridges as sacrificial bonds in interpenetrating network hydrogels, Macromolecules 49 (2016) 4340–4348, https://doi.org/10.1021/acs.macromol.6b00874.
[16] J.-Y. Sun, X. Zhao, W.R.K. Illeperuma, O. Chaudhuri, K.H. Oh, D.J. Mooney, J. J. Vlassak, Z. Suo, Highly stretchable and tough hydrogels, Nature 489 (2012) 133–136, https://doi.org/10.1038/nature11409.
[17] T. Narita, K. Mayumi, G. Ducouret, P. Hébraud, Viscoelastic properties of poly (vinyl alcohol) hydrogels having permanent and transient cross-links studied by microrheology, classical rheometry, and dynamic light scattering, Macromolecules 46 (2013) 4174–4183, https://doi.org/10.1021/ma400600f.
[18] K. Mayumi, A. Marcellan, G. Ducouret, C. Creton, T. Narita, Stress–strain relationship of highly stretchable dual cross-link gels: separability of strain and time effect, ACS Macro Lett. 2 (2013) 1065–1068, https://doi.org/10.1021/mz4005106.
[19] R. Long, K. Mayumi, C. Creton, T. Narita, C.-Y. Hui, Time dependent behavior of a dual cross-link self-healing gel: theory and experiments, Macromolecules 47 (2014) 7243–7250, https://doi.org/10.1021/ma501290h.
[20] S. Rose, A. Dizeux, T. Narita, D. Hourdet, A. Marcellan, Time dependence of dissipative and recovery processes in nanohybrid hydrogels, Macromolecules 46 (2013) 4095–4104, https://doi.org/10.1021/ma400447j.
[21] J. Guo, R. Long, K. Mayumi, C.-Y. Hui, Mechanics of a dual cross-link gel with dynamic bonds: steady state kinetics and large deformation effects, Macromolecules 49 (2016) 3497–3507, https://doi.org/10.1021/acs.macromol.6b00421.
[22] J. Odent, J.-M. Raquez, J.-M. Thomassin, J.-M. Gloaguen, F. Lauro, C. Jérôme, J.-M. Lefebvre, P. Dubois, Mechanistic insights on nanosilica self-networking inducing ultra-toughness of rubber-modified polylactide-based materials, Nanocomposites 1 (2015) 113–125, https://doi.org/10.1179/2055033215Y.0000000005.
[23] G. Kfoury, J.-M. Raquez, F. Hassouna, J. Odent, V. Toniazzo, D. Ruch, P. Dubois, Recent advances in high performance poly(lactide): from "green" plasticization to super-tough materials via (reactive) compounding, Front. Chem. (2013) 1, https://doi.org/10.3389/fchem.2013.00032.
[24] J. Odent, J.-M. Raquez, P. Dubois, Highly toughened polylactide-based materials through melt-blending techniques, in: S. Fakirov (Ed.), Biodegradable Polyesters, Wiley-VCH Verlag GmbH & Co. KGaA, Weinheim, Germany, 2015, pp. 235–274, https://doi.org/10.1002/9783527656950.ch10.
[25] P. Saini, M. Arora, M.N.V.R. Kumar, Poly(lactic acid) blends in biomedical applications, Adv. Drug Deliv. Rev. 107 (2016) 47–59, https://doi.org/10.1016/j.addr.2016.06.014.
[26] U. Meekum, A. Khiansanoi, PLA and two components silicon rubber blends aiming for frozen foods packaging applications, Results Phys. 8 (2018) 79–88, https://doi.org/10.1016/j.rinp.2017.11.030.
[27] H. Zhang, H. Bai, S. Deng, Z. Liu, Q. Zhang, Q. Fu, Achieving all-polylactide fibers with significantly enhanced heat resistance and tensile strength via in situ formation of nanofibrilized stereocomplex polylactide, Polymer 166 (2019) 13–20, https://doi.org/10.1016/j.polymer.2019.01.040.
[28] A. Bouzouita, D. Notta-Cuvier, R. Delille, F. Lauro, J.-M. Raquez, P. Dubois, Design of toughened PLA based material for application in structures subjected to severe loading conditions. Part 2. Quasi-static tensile tests and dynamic mechanical analysis at ambient and moderately high temperature, Polym. Test. 57 (2017) 235–244, https://doi.org/10.1016/j.polymertesting.2016.11.034.
[29] S. Farah, D.G. Anderson, R. Langer, Physical and mechanical properties of PLA, and their functions in widespread applications — a comprehensive review, Adv. Drug Deliv. Rev. 107 (2016) 367–392, https://doi.org/10.1016/j.addr.2016.06.012.
[30] T. Peppel, M. Köckerling, Imidazolium-based Zwitterionic butane-1-sulfonates: synthesis and properties of 4-(1-(2-Cyanoethyl)imidazolium)butane-1-sulfonate and crystal structures of 4-(1-Alkylimidazolium)butane-1-sulfonates (alkyl = methyl, ethyl, propyl), Z. Anorg. Allg. Chem. 637 (2011) 870–874, https://doi.org/10.1002/zaac.201100053.
[31] N.J. Fernandes, T.J. Wallin, R.A. Vaia, H. Koerner, E.P. Giannelis, Nanoscale ionic materials, Chem. Mater. 26 (2014) 84–96, https://doi.org/10.1021/cm402372q.
[32] N.-D. Tien, T.-P. Hoa, M. Mochizuki, K. Saijo, H. Hasegawa, S. Sasaki, S. Sakurai, Higher-order crystalline structures of poly(oxyethylene) in poly(d,l-lactide)/poly (oxyethylene) blends, Polymer 54 (2013) 4653–4659, https://doi.org/10.1016/j.polymer.2013.06.028.
[33] H. Liu, J. Zhang, Research progress in toughening modification of poly(lactic acid), J. Polym. Sci. B Polym. Phys. 49 (2011) 1051–1083, https://doi.org/10.1002/polb.22283.